THE IMPACT OF BUBBLE ARRAYS ON GLASS FLOW AND REDOX STATE OF GLASS DURING GLASS MELTING

LUBOMÍR NĚMEC, MILOŠ JIŘIČKA, JOSEF MATYÁŠ, ALEXANDER FRANĚK*

Laboratory of Inorganic Materials of the Institute of Inorganic chemistry ASCR and the Institute of Chemical Technology, Technická 5, 166 28 Prague, Czech Republic
E-mail: Lubomir.Nemec@vscht.cz

**Glass Service, Rokytnice 60, 755 01 Vsetín, Czech Republic*

Submitted March 27, 2001; accepted September 7, 2001.

The bubble arrays present in the glass melting spaces may extract gases from the melt and thus decrease its refining ability, as well as influence glass flow by changing density of the mixture glass melt-bubbles. Both phenomena were examined using the 3D and 2D models. The examination of the bubble extraction ability on elected glass pathways in the 3D model has shown that refining gases were evidently removed from the reduced glass melt (amber) while the concentration drop of dissolved refining gases in an oxidized glass was negligible. The distinct bubble stirring effect in the 2D melting space was observed when inputting about 3 vol.% of small bubbles ($a = 2.5 \times 10^{-4}$ m) through a part of bottom. The effect of bubble concentration gradients on the intensity of glass convection was analogical to the impact of temperature gradients on glass flow in case of temperature convection. Different behavior was observed, however, when examining the impact of geometrical shape on the melt flow. Both described phenomena should be considered in advanced mathematical models of glass melting spaces.

Keywords: Bubble, Glass flow, Redox state

INTRODUCTION

The results of simplified mathematical models of glass melting show that bubble concentrations in some regions of a glass melting space, namely below the batch blanket and in the area of maximum temperature, may achieve up to tens of volume percents [1]. Such high bubble densities may influence not only glass properties as viscosity, density or effective heat conductivity but also the fundamental melting processes. The bubble arrays are able to evoke the macroscopic glass flow as a consequence of bubble concentration gradients, to extract gases from the melt into atmosphere and to enhance corrosion of materials in contact with the melt. The contemporary mathematical models of the refining process start from the temperature and glass velocity fields valid for the pure melt and ignore therefore the probable mutual interference of the melt and bubbles [1, 2]. This fact makes the model results partially unreliable and their subtle applications e.g. for glass furnace control very problematic. The further model improvement leads to parallel consideration of mentioned effects during calculations, however, such models appear to be rather complicated for operational applications. The process complexity and the need of additional data also discourage from applying this way. The alternative approach offers the separate investigation of various effects and subsequent estimation of their importance under real conditions. Only significant phenomena should be then included into the models. The simplified models of processes may be used here but one must be aware of their limited ability when transferring results to different conditions.

This work aims at the separate examination of mutual interference between bubble arrays and glass flow, as well as redox state of glass. The partial models developed by authors of this article and by their co-workers were applied to find the solution of the problems.

THEORETICAL

To study the impact of bubbles on the redox state of glass, the 3D Glass Model was used [3], making it possible to acquire the pure glass melt temperature and velocity field in a melting furnace under given boundary conditions. Both value fields served as a base for the *ex post* calculation of the redox component distribution inside the space [4]. The bubble density distribution in the melting space was also obtained by applying the *ex post* calculation procedure too [1, 5]. The mentioned procedure used the temperature, velocity and redox component concentration fields of the pure glass melt to calculate the pathways of bubble representatives through the model melting space and to provide subsequently the bubble concentrations in the steady state. When examining the bubble influence on the glass flow, the 2D model was constructed [6] to describe the mutual impact of monodisperse particles and a glass melt under isothermal conditions.

Calculation conditions

In the 3D modeling, the rectangular melting space with throat was 16.5 m long and 4 m wide. The glass melt layer thickness was 1 m. The temperature maximum 1500 °C was at X = 5.5 - 6.5 m and the throat was 10.5 m located from the front wall. When studying the bubble and glass flow interference, the 2D model melting space 1 × 1 m was chosen for most calculations. The bubbles entered the space by the central part of the bottom. The glass was the soda-lime-silica glass containing 74 wt.% SiO_2, 16 wt.% Na_2O and 10 wt.% CaO. The glass melt was refined by the sodium sulfate. The glass temperature as well as velocity fields and subsequently, the redox distribution and bubble distribution in the space were calculated using the above mentioned partial models. The bubble impact on the redox state of glass was examined along glass melt pathways through the melting space. The pathways have started under the glass batch blanket and finished in the throat. The local values of the bubble number density, gas concentrations in the melt and in bubbles were used to calculate the local mass flow of refining gases between the bubbles present and the melt (see equation (1) in [5]). The sum of concentration changes of refining gases along elected pathways gave the approximate concentration decrease of the refining agent concentration in the melt owing to bubbles. The accuracy of results was limited by the fact that the local mass flow did not take into account the previous effect of bubbles. The typical values of volume fractions of bubbles in the melt were obtained also for usage in the 2D model. In the latter 2D model calculations, the bubbles of constant radii 2.5×10^{-4}, 5×10^{-4} and 1×10^{-3} m and in volume concentrations 0.2, 1, 3, 10, 20 and 30 vol.%, respectively, were used to calculate the resulting bubble and glass velocity distribution in the space. Bubbles entered the central part of the bottom space and the fraction of bottom occupied by inputting bubbles moved from 0.02 to 1, but in most cases was fixed at 0.02.

The following calculations were executed to elucidate the outlined problems:

- the decrease of the refining agent concentration along forty typical pathways of the melt through the 3D melting space
- the dependence between the characteristic velocity of the melt flow in the 2D space and:
  - the initial volume concentration of bubbles in the melt, ϑ_o
  - the fraction of bottom occupied by inputting bubbles, X/X_o
  - the bubble radius, a
  - the shape of the space, Y_o/X_o
  - the density difference of bubbles and melt, $\rho_{gl} - \rho_{bub}$
  - the kinematic glass viscosity, υ

RESULTS OF CALCULATIONS

A typical picture of extraction of the dissolved SO_2 from the flat glass melt containing sodium sulfate as the fining agent along 4 glass trajectories is plotted in figure 1*a*, the similar dependence valid for the same glass containing sulfides (amber glass) is presented in figure 1*b*. The concentration drops in figure 1*a* corresponds to short residence times of glass in the high temperature region near the glass surface. The repeated concentration steps express the glass circulation in the melting region. The concentration of the dissolved SO_2 decreased along all pathways examined, nevertheless, the maximum concentration drop did not exceed 3 mol m^{-3}. In the reduced glass, on the contrary, the bubble extraction ability is much higher attaining up to tens of mols of SO_2 per m^3 as shown in figure 1*b*.

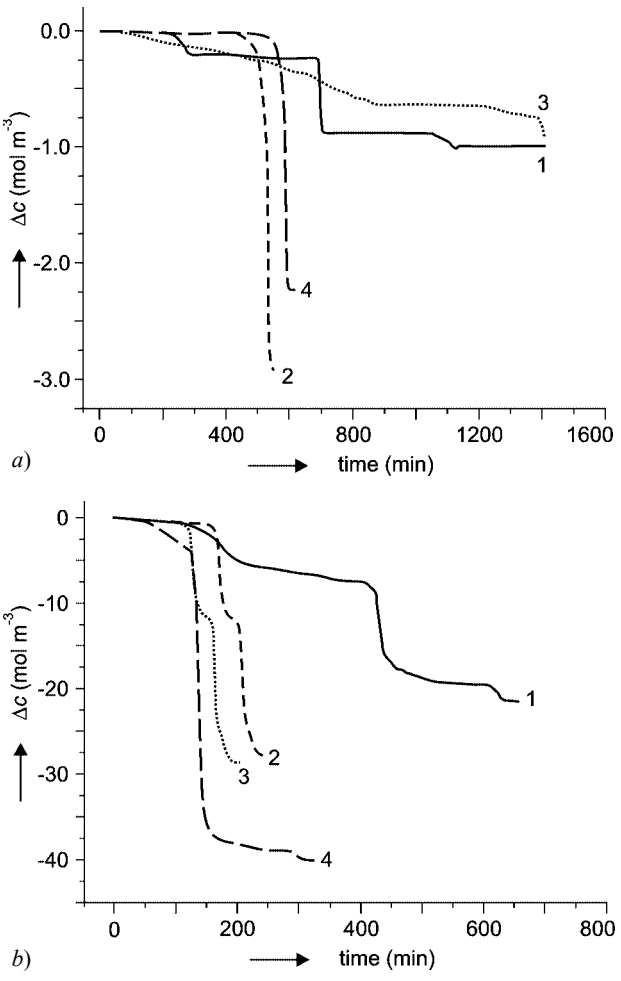

Figure 1. The concentration drop of the dissolved SO_2 along four typical glass pathways through the melting region. The concentration drop was brought about by the extraction effect of bubbles.
a) oxidized glass containing sodium sulfate, *b*) amber glass.
1 - 4: bubble trajectories.

The values of the glass volume occupied by bubbles in the 3D model may give an approximate information about bubble concentration gradients in the space. The concentration differences are the driving force of convection due to bubbles and help us to provide the 2D model with the appropriate input values. The independent calculations of glass flow and bubble density distribution in the 3D model, however, make the results only qualitative. The example of the bubble distribution on two transversal straight lines through the space show nevertheless both high bubble concentrations and bubble concentration gradients, particularly in the region of the temperature maximum close to the glass surface. The impact of bubbles on glass flow appears therefore highly probable. The appropriate dependencies are plotted in figure 2.

The picture of a typical glass velocity distribution in the 2D space is presented in figure 3*a*, *b*. The bubbles entered the central part of the bottom, the fraction of the bottom occupied by inputted bubbles was X/X_o where X_o was the space width. As is obvious from both figures, the glass with bubbles rose through a relatively narrow central vertical column to the glass level and then reversed back to the bottom with a much lower velocity. The fraction of the bottom occupied by bubbles only slightly influenced the character of the flow as the bottom backflow "swept" the inputting bubbles into the narrow rising column of glass at higher values of X/X_o (see figure 3*b*). The characteristic glass velocity and the

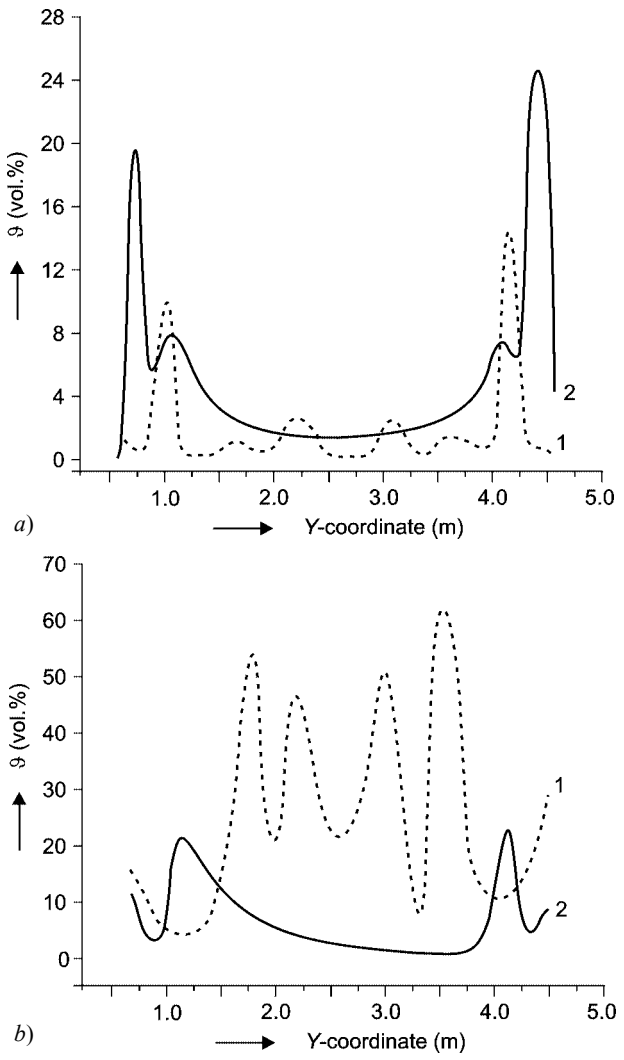

Figure 2. The dependence between the volume concentration of bubbles, ϑ, and Y coordinate in the tranversal sections through the 3D melting space; *a*) X = 1.5 m (under the batch blanket), 1: 0.2 m under the boundary glass batch - glass melt, 2: 0.5 m under the boundary glass batch - glass melt; *b*) X = 6.5 m (in the temperature maximum), 1: 0.2 m under the glass level, 2: 0.5 m under the glass level.

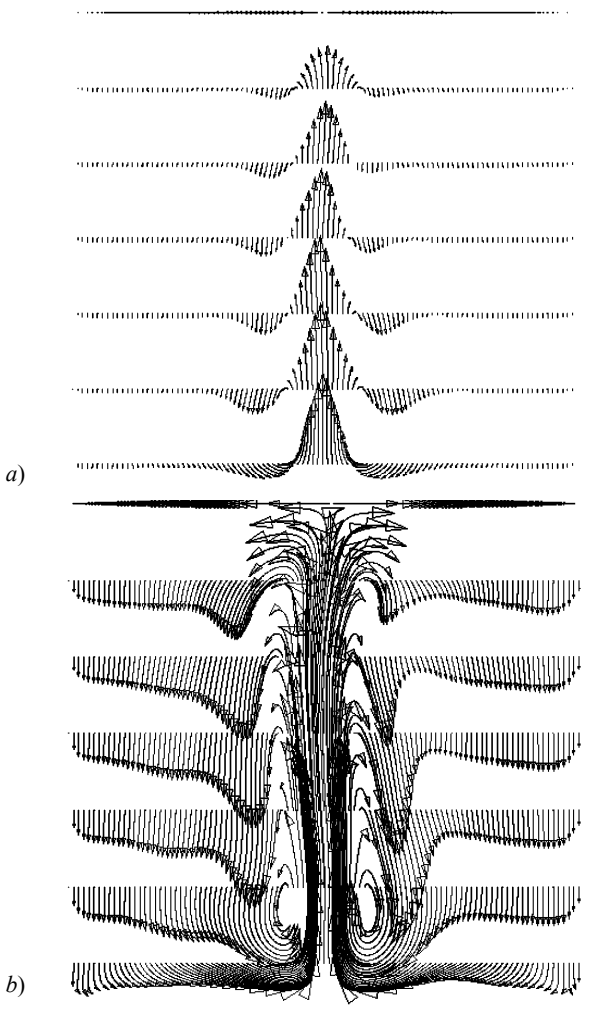

Figure 3. The pictures of two typical glass velocity distributions in the 2D melting space 1 × 1 m. The length of arrows corresponds to the distance run in the course of 10 s. At 1300 °C, the initial bubble volume fraction, ϑ_o = 3 vol.%, the bubble radius $a = 5 \times 10^{-4}$ m, τ = 50 hrs; *a*) the fraction of the bottom occupied by inputting bubbles, X/X_o = 0.02; *b*) the fraction of the bottom occupied by inputting bubbles, X/X_o = 0.5.

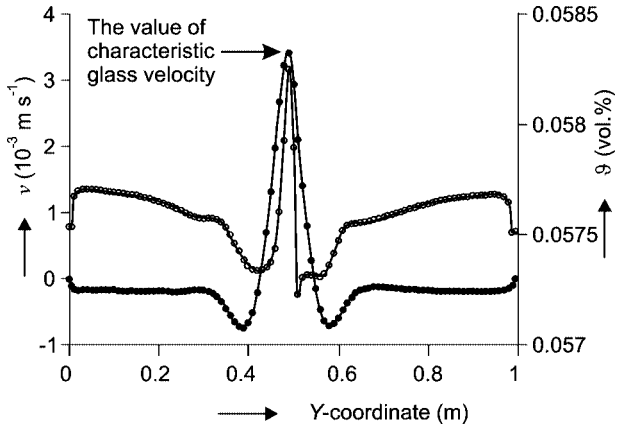

Figure 4. The course of the glass velocity and bubble concentration in a typical case on the line $Y = 0.5$ m and after 50 hrs, at 1300 °C, $\vartheta_o = 3$ vol.%, $X/X_o = 0.02$, $a = 5 \times 10^{-4}$ m. The values of v and $d\vartheta/dX$ in the central part of the curve define the characteristic glass velocity and the characteristic bubble concentration gradient, respectively.
● - velocity, ○ - volume concentration of bubbles

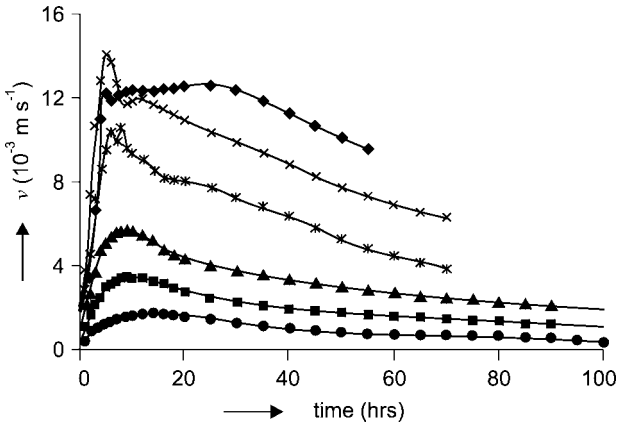

Figure 5. The time development of the characteristic glass velocity for the different values of the initial bubble volume fraction, ϑ_o, at 1300 °C, $X/X_o = 0.02$, $a = 5 \times 10^{-4}$ m.
● - ϑ_o = 0.2 vol.%, ■ - ϑ_o = 1 vol.%, ▲ - ϑ_o = 3 vol.%, ✱ - ϑ_o = 10 vol.%, × - ϑ_o = 20 vol.%, ◆ - ϑ_o = 30 vol.%

characteristic bubble concentration gradient were found to evaluate the results of calculations. The average glass velocity in the central rising glass column and at $Y = 0.5$ m was determined as the characteristic glass velocity. This is apparent from figure 4, where the velocity distribution is plotted on the line $Y = 0.5$ m. The characteristic bubble concentration gradient was read from the steepest central part of bubble concentration curve at identical Y coordinate (see also figure 4). The almost constant concentration of bubbles close to the borders of modeled space indicates the considerable stirring ability of bubbles. This also illustrates the increase of the average bubble concentration with time (see below).

The development of the characteristic glass velocity with time is shown in figure 5. In all cases examined, the velocity grew to the maximum value reached after approximately 10 - 20 hours and subsequently slowly decreased approaching the steady value. However, the steady value was not attained even after 100 hours and similar character of the dependencies between the characteristic glass velocity and time, and the characteristic concentration gradient and time, indicated the approximate proportionality between both characteristic values as seen from figure 6.

The influence of the initial bubble volume concentration on the average characteristic glass velocity and on the average bubble concentration gradient (5 - 50 hours) is demonstrated in figure 7. The initial steep increase of both characteristic values slows down at higher bubble concentrations and in case of the concentration gradient achieves the almost constant value at $\vartheta_o \rangle 20$ vol.%, i.e. the driving force of the glass flow does not grow at higher bubble concentrations. The

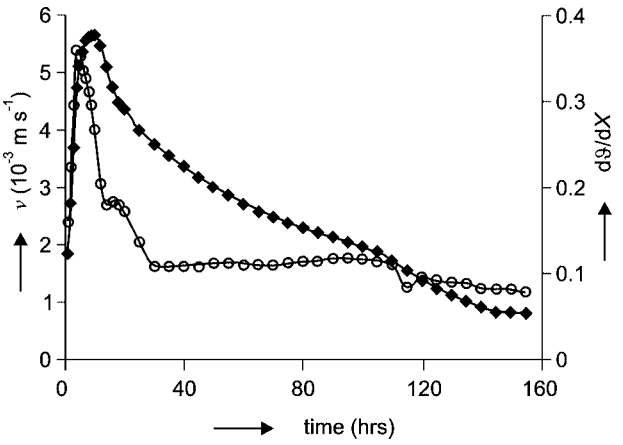

Figure 6. The time development of the characteristic glass velocity and the characteristic bubble concentration gradient at 1300 °C, $\vartheta_o = 3$ vol.%, $X/X_o = 0.02$, $a = 5 \times 10^{-4}$ m.
◆ - velocity, ○ - concentration gradient

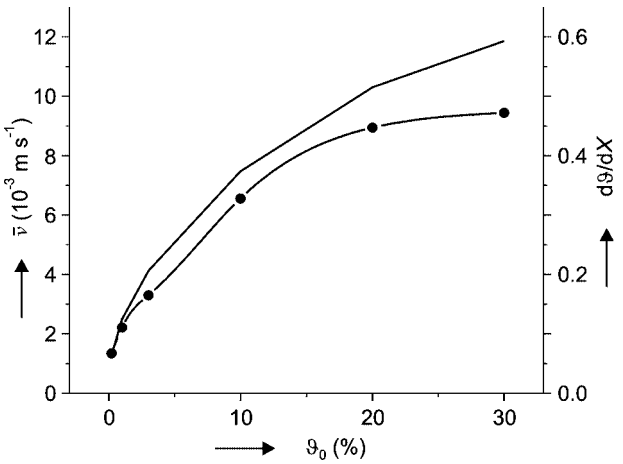

Figure 7. The dependence of the average characteristic glass velocity and the average bubble concentration gradient (5 - 50 hrs) on ϑ_o, at 1300 °C, $X/X_o = 0.02$, $a = 5 \times 10^{-4}$ m.
—— - velocity, ● - $d\vartheta / dX$

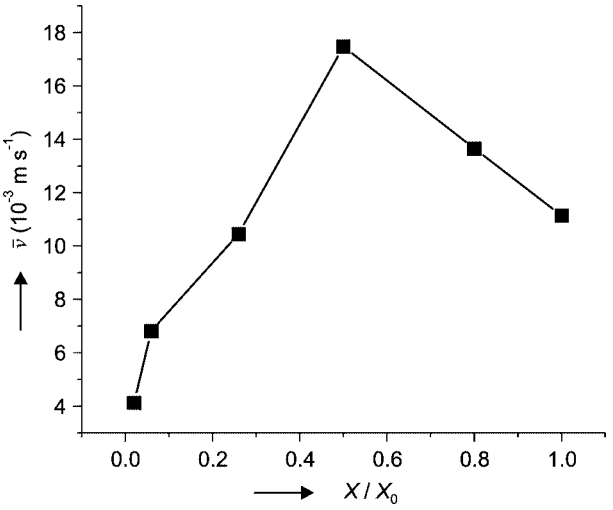

Figure 8. The dependence of the average characteristic glass velocity on the part of bottom occupied by bubbles, X/X_o, at 1300 °C, ϑ_o = 3 vol.%, $a = 5 \times 10^{-4}$ m, τ = 100 hrs.

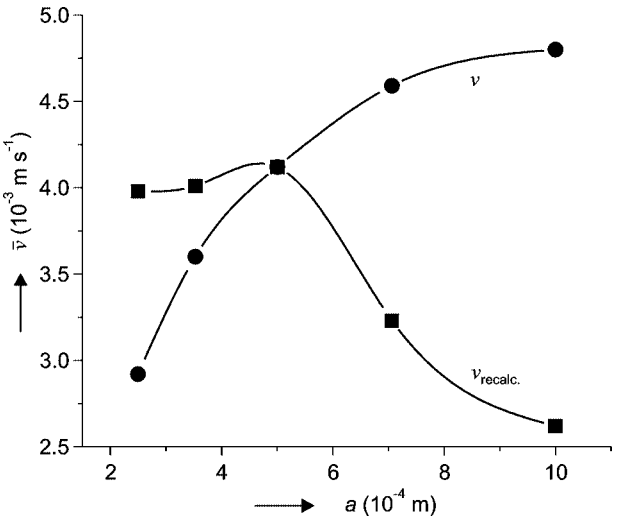

Figure 9. The dependence of the average characteristic glass velocity and the recalculated characteristic glass velocity (5 - 50 hrs) on the bubble radius, a, at 1300 °C, ϑ_o = 3 vol.%, X/X_o = 0.02.

dependence between the average characteristic glass velocity and the fraction of the bottom occupied by inputting bubbles (figure 8) shows, on the contrary, the maximum at about X/X_o = 0.5. The initial velocity growth is brought about by the increasing amount of inputting bubbles, the velocity fall at high occupation values is caused by the changing character of glass flow (disintegration of circulation flows).

Figure 9 presents the dependence of the average characteristic glass velocity on the bubble radius, a. Figure 9 shows also the values of the velocity, recalculated to the standard bubble concentration gradient at $a = 5 \times 10^{-4}$ m. The anticipated independence of $\bar{v}$ on the recalculated standard value of bubble concentration gradient is preserved up to about $a = 5 \times 10^{-4}$ m, then the values $\bar{v}$ decrease. The reason of this decline is not clear but the values of the characteristic bubble concentration gradient of higher a values probably do not represent the driving force of glass flow reliably.

Two relations between the characteristic glass velocity and the space shape were examined, namely the dependence on the space height, Y_o, for the constant X_o = 1 m, and on the Y_o/X_o ratio for the constant space volume (X_oY_o = 1 m^2). Both dependencies are plotted in figure 10. To complete the parametrical study, the effect of the density difference between glass and bubbles,

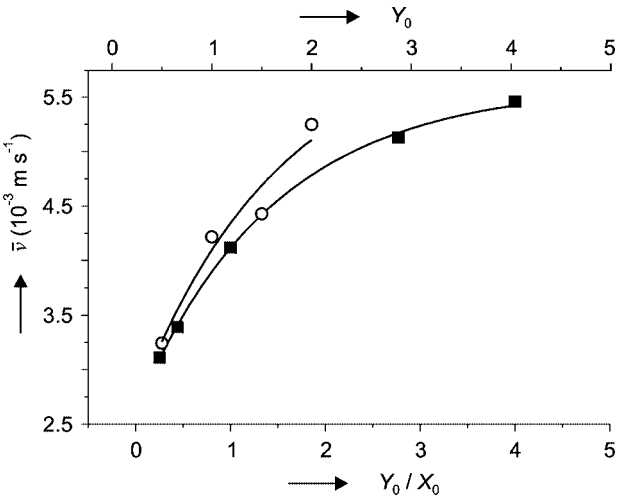

Figure 10. The dependence of the average characteristic glass velocity on the geometrical shape of the space, at 1300 °C, ϑ_o = 3 vol.%, $a = 5 \times 10^{-4}$ m.
○ - the dependence on the Y_o at constant X_o = 1 m, ■ - the dependence on the Y_o/X_o at constant X_oY_o = 1 m^2.

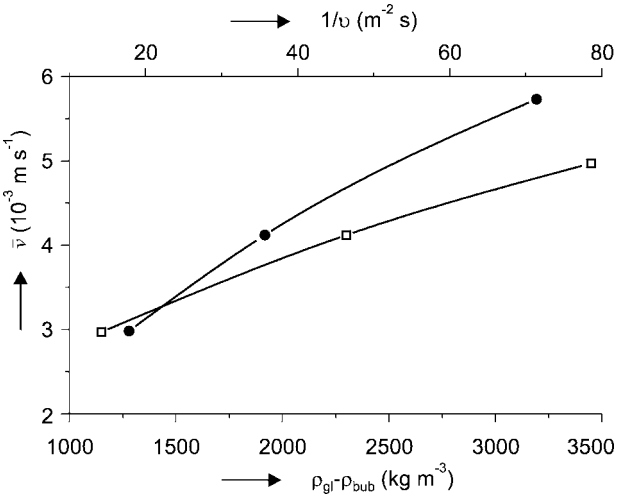

Figure 11. The dependence of the average characteristic glass velocity on the density difference, $\rho_{gl} - \rho_{bub}$, and the reciprocal value of kinematical viscosity, $1/\upsilon$. □ - the dependence on the density difference, ● - the dependence on the reciprocal value of glass kinematical viscosity.

ρ_{gl} - ρ_{bub}, and the reciprocal value of kinematical viscosity of glass, $1/\upsilon$, on the average characteristic glass velocity are plotted in figure 11.

DISCUSSION

The temperature stability of sulfates and sulfides in the glass is responsible for the different bubble extraction ability in the oxidized glass melts with the sodium sulfate and in the reduced glass containing sulfides. As sulfate ions decompose apparently only above 1400 °C, the small part of glass trajectories is exposed to gas diffusion into extracting bubbles and consequently, the concentration decrease of sulfates is low. Figure 12 a presenting the concentration difference distribution for the examined 40 trajectories shows the maximum frequency at $\Delta c \in \langle 0;0.3 \rangle$ (mol m^{-3}). The bubble clouds in glasses containing sulfates should therefore influence the resulting redox state of glass only very slightly. The reciprocal temperature dependence of sulfides stability, on the contrary, shifts the production of SO_2 and consequently, the SO_2 extraction by bubbles, towards lower temperatures. That is why the bubble extraction ability along predominantly low temperature pathways is high. The concentration drop distribution for 40 trajectories examined exhibits the maximum frequency at $\Delta c \in \langle 40;45 \rangle$ (mol m^{-3}) (see figure 12*b*). As the concentration of the refining agent in the melt is of the same order of magnitude as Δc, the distinct influence of bubbles on the redox state of glass in reduced glasses containing sulfides can be expected. The glass flow intensity and bubble concentration distribution acquired from the 2D model show that even a small amount of bubbles entering the space stirs the melt vigorously (see figures 3 and 4). It appears to be useful to compare the stirring effect of bubbles with an ideal mixer in the same 2D space.

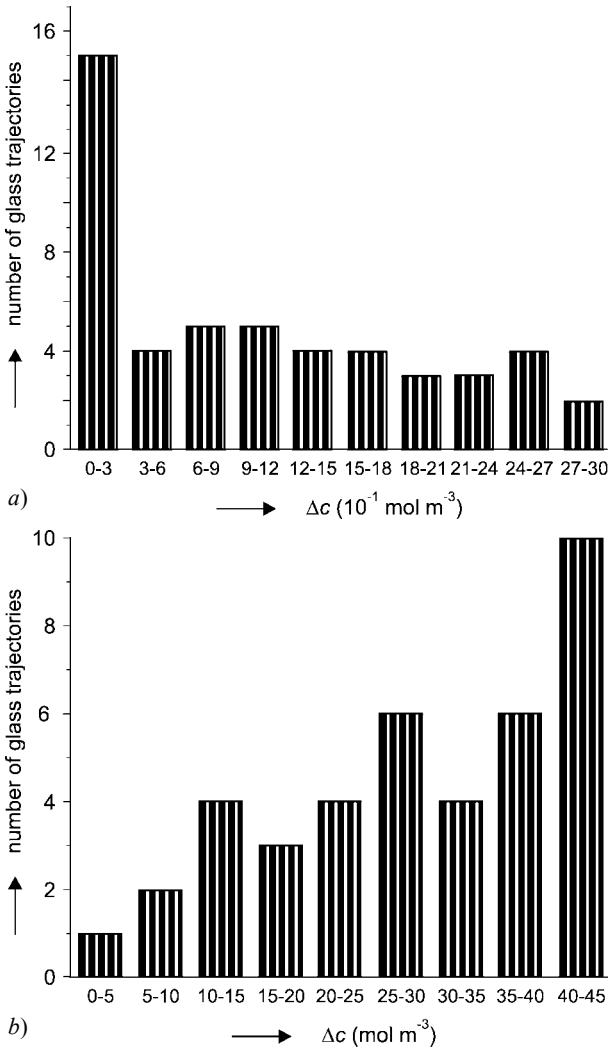

Figure 12. The concentration difference distribution for 40 examined glass trajectories in the glass melt containing sulfate ions or in the amber glass containing sulfide ions;
a) soda-lime-silica glass containing sulfate ions, *b*) amber glass containing sulfide ions.

The bubble concentration change brought about by the inputting bubbles is given by:

$$\mathrm{d}\vartheta^{+} = \frac{X}{X_o}\, u\vartheta_o\, \mathrm{d}\tau \tag{1}$$

where u is the bubble rising velocity. The bubble concentration decrease by bubbles leaving the space through the level describes the equation:

$$\mathrm{d}\vartheta^{-} = u\vartheta\, \mathrm{d}\tau \tag{2}$$

As $\mathrm{d}\vartheta = \mathrm{d}\vartheta^{+} + \mathrm{d}\vartheta^{-}$, the resulting bubble concentration change can be expressed by the equation:

$$\vartheta^{+} = \frac{X}{X_o}\, \vartheta_o\, [1 - \exp(-u\tau)] \tag{3}$$

Equation (3) shows that under condition of ideal mixing, the increase in the relative bubble concentration depends only from the bubble rising velocity (i.e. from the bubble radius). The final bubble concentration in the space attains the value $X/X_o\vartheta_o$ ($\tau \to \infty$). The almost ideal mixing of the melt is confirmed by the fact that courses of equation (3) for two values of bubble rising velocities almost coincide with the bubble concentration increase, calculated from the 2D model. The results of this comparison are presented in figure 13.

The characteristic concentration gradient of bubbles is considered the driving force of glass convection flow. Figure 14 illustrates the linear dependence between the two average characteristic values. The character of this dependence is similar to the relation between the horizontal glass velocity and temperature gradient in a rectangular space, presented by Cooper [7]:

$$v_x = \frac{\alpha g}{\upsilon}\, \frac{\mathrm{d}T}{\mathrm{d}X}\, Y_o^3\, \mathrm{f}(Y) \tag{4}$$

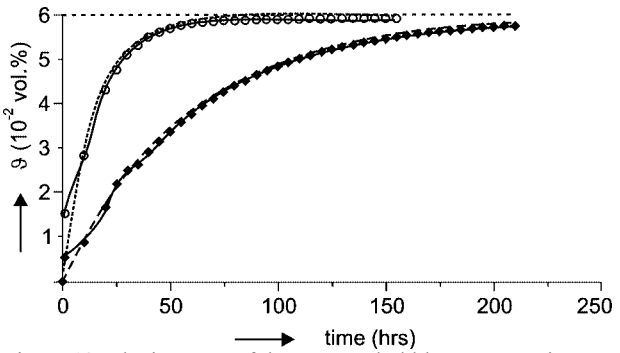

Figure 13. The increase of the average bubble concentration, ϑ, in the space as a function of time at 1300 °C, ϑ_o = 3 vol.%, X/X_o = 0.02.
- - - - - c (final value); ○ - v = 1.91 × 10^{-5} m s^{-1}, a = 5 × 10^{-4} m; . . . . v = 1.91 × 10^{-5} m s^{-1}, equation (3); ◆ - v = 4.78 × 10^{-6} m s^{-1}, a = 2.5 × 10^{-4} m; — — — v = 4.78 × 10^{-6} m s^{-1}, equation (3)

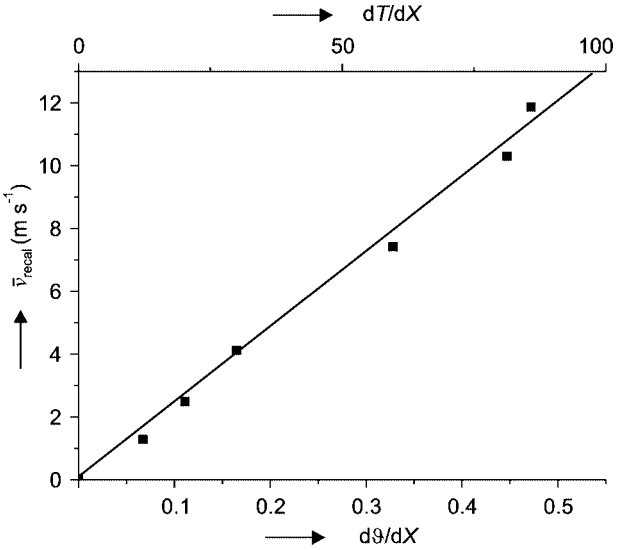

Figure 14. The dependence between the average characteristic glass velocity and the average bubble concentration gradient at 1300 °C, X/X_o = 0.02, a = 5 × 10^{-4} m.

where α is the volume thermal expansion coefficient of glass, T is temperature, Y_o is the height of the glass layer, υ is the kinematic viscosity of glass and f(Y) is a simple function of the vertical coordinate. The corresponding values of the temperature gradients, dT/dX are also presented in figure 14, showing that driving forces caused by bubbles in the 2D model correspond approximately to those in commercial glass melting furnaces. This fact indicates that temperature and concentration convection have similar impact on the glass flow in glass melting furnaces.

The similarity between temperature and concentration convections is further illustrated by linear dependence between the average characteristic glass velocity, recalculated to the standard concentration gradient (ϑ_o = 3 vol.%, dϑ/dX = 0.165), and the glass and gas density difference (which corresponds to α in equation (4)), as well as between the characteristic glass velocity and the reciprocal value of the kinematic viscosity. Both dependences are presented in figure 15. Different behavior is, however, apparent from figure 16 where the approximately linear dependence between the characteristic glass velocity, recalculated to the standard concentration gradient (ϑ_o = 3 vol.%, dϑ/dX = 0.165), and $Y_o^{1/2}$ (X_o = 1 m), respectively $(Y_o/X_o)^{1/4}$ (X_oY_o = 1 m^2) can be found. The cubic character of the dependence between the glass velocity and the height of glass layer

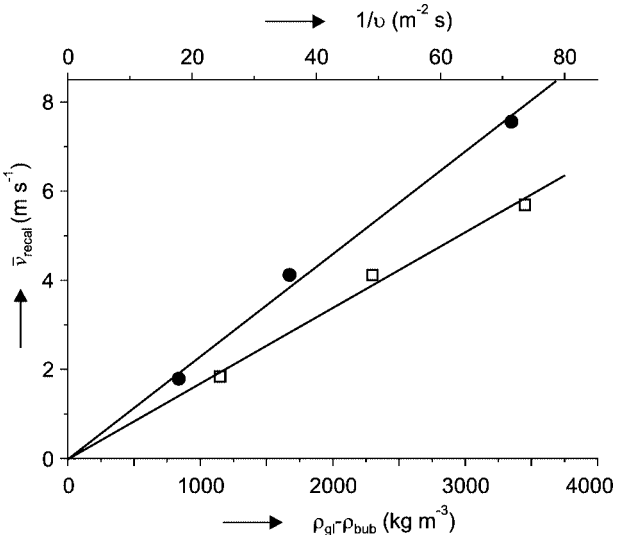

Figure 15. The dependence between the average characteristic glass velocity, recalculated to the standard concentration gradient (ϑ_o = 3 vol.%, dϑ/dX = 0.165), and the glass and gas density difference, as well as the reciprocal value of the kinematical viscosity of glass. □ - 1/υ, ● - ρ_{gl} - ρ_{bubl}

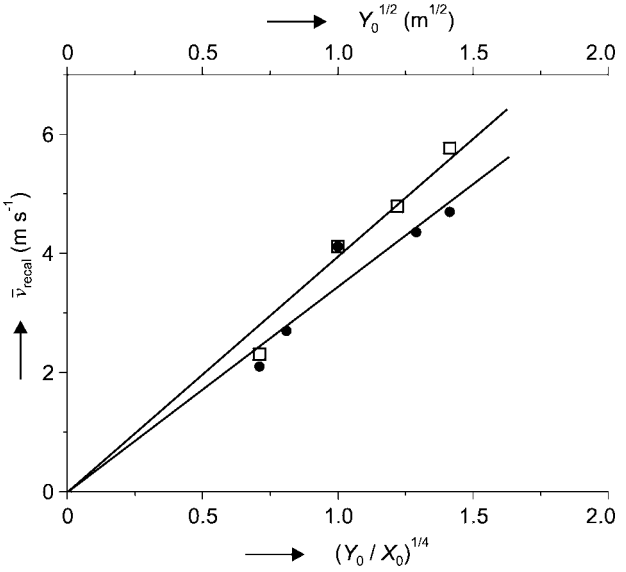

Figure 16. The dependence between the average characteristic glass velocity, recalculated to the standard concentration gradient (ϑ_o = 3 vol.%, dϑ/dX = 0.165), and the value $Y_o^{1/2}$ (● - X_o = 1 m), as well as $(Y_o/X_o)^{1/4}$ (□ - X_oY_o = 1 m^2).

is, on the contrary, characteristic for the temperature convection (see equation (4)).

Taking into account the revealed relations between the characteristic glass velocity and examined initial and boundary parameters, the following semiempirical relation, based on results of presented 2D model may be written for the given 2D space with constant value of X_o:

$$\overline{v} = \text{const} \ \frac{\Delta\rho g}{\upsilon} \ \frac{\mathrm{d}\vartheta}{\mathrm{d}X} \ Y_o^{1/2} \qquad (5)$$

In agreement with temperature convection, the intensity of glass flow is directly proportional to the density differences and horizontal convection gradient, and indirectly proportional to the glass viscosity. A dissimilarity of both cases was found when calculating the significance of the height of glass layer, possibly the impact of geometrical shape on the glass flow. The significance of the height of glass layer was found much lower for the concentration convection being expressed by a proportionality between the characteristic glass velocity and the square root of the height (see equation (5)), whereas the same dependence for the temperature convection was cubic (see equation (4)). One of reasons of this behavior may be differences in nature of both phenomena: the space walls exhibit heat losses but no particles could penetrate through the walls. A relatively complicated relation was found between mixture flow and the portion of the bottom occupied by inputting bubbles (see figure 8). It is apparent from the nature of the model that the concentration convection should be absent when $X/X_o = 0$ and should have only low intensity when $X/X_o = 1$, i.e. when the flow is evoked only by the requirement of flow continuity. Figure 8 confirms this assumption, however, no simple relation between the average characteristic glass velocity and parameter X/X_o was revealed.

CONCLUSION

Two phenomena seem to influence the results of contemporary mathematical models of glass melting spaces: refining gas extraction from the melt by rising bubbles and glass melt flow, caused by horizontal bubble concentration gradients. Refining gases may be extracted by bubbles in the regions of high bubble densities, this influence being significant especially for refining agents working at lower and medium temperatures (SO_2 extracted by bubbles from amber glass). The horizontal bubble concentrations gradients, present in commercial glass furnaces, evoke the glass flow having at least the same intensity as flow caused by temperature convection. Analogy between temperature convection and concentration convection in the 2D melting space was found as for the effect of bubble concentration and temperature gradients. Further confirmation of the latter bubble effect by using 3D model is needed. Both phenomena should be considered in the appropriate mathematical models of glass melting spaces.

Acknowledgement

This work was supplied with the subvention by Grant Agency of AS CR, Project No. S4032103.

References

1. Matyáš J., Němec L., Jiřička M., Franěk A.: Proc. Int. Conference Glass in the New Millenium: Challenges and Break-through Technologies, Amsterdam, May 15-19, 2000.
2. Němec L., Kloužek J., Schill P., Ullrich J.: Proc. Int. Conference on Fundamentals of Glass Science and Technology, p. 340, Växjö, June 9 - 12, 1997.
3. Schill, P.: Proc. 2nd International Seminar on Mathematical Simulations in the Glass Melting, p.102, Vsetín, Czech Republic, May 15 - 19, 1993.
4. Němec L., Raková M.: Ceramics - Silikáty *42*, 1 (1998).
5. Kloužek J., Matyáš J., Němec L., Trochta M., Ullrich J.: Proc. 5th ESG Conference Glass Science and Technology for the 21st Century, p.A2, Prague, Czech Republic, June 19 - 24, 1999.
6. Kloužek J., Franěk A.: Ceramics-Silikáty *45*, 70 (2001).
7. Cooper A. R.: A Collected Papers of the XIV Int. Congress on Glass, p.1, New Delhi 1986.

VLIV SOUBORŮ BUBLIN NA PROUDĚNÍ SKELNÉ TAVENINY A JEJÍ OXIDAČNĚ REDUKČNÍ STAV BĚHEM TAVICÍHO PROCESU

LUBOMÍR NĚMEC, MILOŠ JIŘIČKA, JOSEF MATYÁŠ, ALEXANDER FRANĚK*

Laboratoř anorganických materiálů, společné pracoviště AV ČR a VŠCHT v Praze, Technická 5, 166 28 Praha

**Glass Service, Rokytnice 60, 755 01 Vsetín*

Soubory bublin přítomné v tavicím prostoru během tavicího procesu skel extrahují a vynášejí k hladině čeřící plyny rozpuštěné v tavenině a snižují schopnost taveniny odstraňovat bubliny. Snižují rovněž průměrnou hodnotu hustoty směsi tavenina – bubliny a mohou vyvolat proudění skloviny. Oba jevy byly zkoumány s použitím 2D a 3D modelů. Sledování extrakce plynů bublinami na vybraných trajektoriích skelné taveniny v 3D tavicím prostoru ukázaly, že rozpuštěné plyny byly zřetelně extrahovány bublinami v redukovaném skle obsahujícím sirníkové ionty, zatímco stejný efekt u skla obsahujícího síranové ionty byl zanedbatelný. S použitím 2D modelu byl prokázán výrazný efekt malého množství bublin (3 obj.% malých bublin vstupujících částí dna prostoru) na proudění v izotermním prostoru. Byla zjištěna analogie mezi vlivem horizontálních teplotních a koncentračních gradientů na přirozenou konvekci skelné taveniny. Vliv výšky tavicího prostoru na intenzitu proudění taveniny byl podstatně méně výrazný v případě koncentrační konvekce. Oba vlivy bublin na chování taveniny je třeba uvažovat při matematickém modelování tavicích částí sklářských pecí.